



OPEN

A remarkable permeability enhancement of $\text{Ni}_{1-x}\text{Zn}_x\text{Fe}_2\text{O}_4$ ($x = 0.65$ and 0.70), using a multi-compound calcined additive

S. Shatooti & M. Mozaffari✉

In this study, entanglement of composition, additive and/or sintering conditions and their effects on magnetic properties of soft ferrites, nickel zinc spinel ferrites ($\text{Ni}_{1-x}\text{Zn}_x\text{Fe}_2\text{O}_4$, $x = 0.65$ and 0.70) which were prepared via conventional solid-state reaction method investigated. Also an equiponderant calcined mixture of Bi_2O_3 , CaO , CeO_2 , SiO_2 , Al_2O_3 , Y_2O_3 and nanotitania was mixed thoroughly and used as a multi-compound calcined additive (MCCA). Calcined ferrite powders were crushed, dry and wet milled, dried, mixed with different amounts of MCCA (0.0, 0.5, 1.0, 1.5 and 2.0 wt%), formed in toroidal shapes and finally sintered at different temperatures, from 1150 up to 1360 °C for 3 h. X-ray diffraction assessment confirmed formation of the single phase cubic spinel structures. Initial permeability and Q-factor spectra of the toroids were obtained from 0.1 to 1000 kHz, using an LCR meter. The results show that initial permeability of each sample has a maximum and addition of MCCA to the ferrites leads to a marvelous increase in permeabilities. Additionally, MCCA decreases the optimum sintering temperature too. The optimum amounts of additive were 1.0 and 0.5 wt% for the $x = 0.65$ ($\mu' = 492$, $T_s = 1280$ °C) and $x = 0.70$ ($\mu' = 478$, $T_s = 1320$ °C), respectively. Permeability spectra illustrate that utility zone of the $\text{Ni}_{0.35}\text{Zn}_{0.65}\text{Fe}_2\text{O}_4$ and $\text{Ni}_{0.3}\text{Zn}_{0.7}\text{Fe}_2\text{O}_4$ are both less than 100 and 10 kHz, respectively. The results represent that there is a strong entanglement between composition, additive and/or sintering conditions. It can be concluded the MCCA added $\text{Ni}_{0.35}\text{Zn}_{0.65}\text{Fe}_2\text{O}_4$, is suitable for application in the switching power supplies.

Keywords Ni–Zn ferrite, Solid-state reaction, Sintering process, Multi compound calcined additive (MCCA), Initial permeability

Nowadays, ceramics due to their stronger ionic or covalent bonding than metals have attracted a great deal of attentions and applications in various fields such as; electronic industry, high temperature superconductors, automotive engines, and medical implants^{1,2}. Ferrites as non-conductive ceramics have been investigated and hired in electronic and electric devices due to high electrical resistivity, high chemical stability, and their applicable frequency-dependent permittivity and permeability in the radio frequency (RF) region^{3,4}. Spinel ferrites with cubic crystal structure, with the $\text{Fd}\bar{3}\text{m}$ space group, are expressed by the general chemical formula MFe_2O_4 , where M is a divalent cation such as Fe^{2+} , Mn^{2+} , Ni^{2+} , Zn^{2+} , Co^{2+} , ... or combinations of the different cations with a resultant valence of two. They have been extensively utilized in different field of technology such as electronic and communicating devices, catalyst, drug delivery, gas sensors, magnetic hyperthermia and etc.^{5–8}.

At low frequencies (< 100 kHz), ferrites are used as core of inductors in low pass LC filters. Due to their high permeability and high resistivity, which in turns result in low eddy current loss at high frequencies (> 100 kHz), ferrites have been extensively used in electromagnetic devices e.g., antenna rods, cores in chock coils, inductors and transformers^{9–11}. Thereupon, Ni–Zn ferrites as mixed spinel soft-magnets are appropriate candidates for applications from MHz to GHz frequencies, due to their high resistivity^{12,13}. In addition, it has capability to absorb electromagnetic radiation at high frequencies, which is representing it as an appropriate material for magnetic absorbers in electronic devices¹⁴.

Department of Physics, Faculty of Physics, University of Isfahan, Isfahan 81746-73441, Iran. ✉email: mozaffari@sci.ui.ac.ir

Ni–Zn ferrites with various amounts of zinc content and different dopants, prepared via different synthesis routes such as; sol–gel, co-precipitation, hydrothermal and conventional ceramic technique in diversity of conditions have been perused and reported^{15–19}. The magnetic and electrical properties of Ni–Zn ferrite like to other ferrites is considerably dependent on cation distribution and microstructure, which in turn depend on preparation path and starting materials^{20,21}.

In the ceramic industry, the conventional ceramic technique is a common synthesis route, because of availability and low cost starting reagents. In this route, proper stoichiometric amounts of oxides or carbonates of metals, as raw materials, are thoroughly wet and/or dry mixed and calcined to get desired phase. The calcined powders are crushed and milled to get submicron particles and formed into desired shapes. After that the shaped sample is sintered at relatively high temperatures to get final density and microstructure²². Solid-state sintering occurs when the compacted powders (green body) are heated at temperatures below the melting points of each component. Sintering is a key step in the solid-state reaction in the preparation and production of ferrites, which it in turns affect the microstructure, electric and magnetic properties of the final products²³.

Additionally, in the so-called additive sintering a small amount of insoluble substance or a combination of substances are used, which influence magnetic and electrical properties and/or microstructure of ferrites by different mechanisms^{24–26}. In high frequency ferrites' preparation, it is required to use at least one additive. There are three categories of additives as follow: first group comprises additives which segregate on the grain boundaries and affect the grain-boundary resistivity, e.g. SiO₂ and CaO. The second ones include additives that improve microstructure during sintering via liquid phase formation, such as Bi₂O₃. The third group encompasses additives which are solved into the grains and modify the magnetic properties, e.g. TiO₂²⁷.

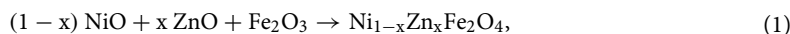
In this work, the effects of a multi-compound calcined additive (MCCA), including equiponderant CaO, CeO₂, SiO₂, Al₂O₃, Y₂O₃, nanotitania and Bi₂O₃, in which the last one is doubled in weight, on the sintering temperatures and permeabilities of Ni_{1-x}Zn_xFe₂O₄ (x = 0.65 and 0.70) were investigated and compared with those of the additive-free samples.

Experimental Synthesis procedure

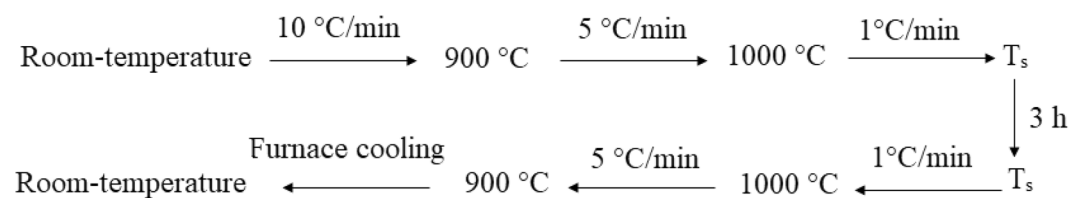
Fe₂O₃ (from a domestic source with minimum purity of 99.5%), NiO (with minimum 75% Ni content, Merck Co., Germany), ZnO (99.5%, Merck Co., Germany), Bi₂O₃ (99%, Merck Co., Germany), CaO (99.9%, Sigma Aldrich), CeO₂ (99% from Scharlau), SiO₂ (from a domestic source with minimum purity of 99%), nanotitania (99%, Teconan), Y₂O₃ (99%, Riedel-Deltaen) and Al₂O₃ (99.99%, Merck Co., Germany) were used as starting materials.

To investigate the effect of a multi compound additive on the permeability and sintering temperature of the Ni_{1-x}Zn_xFe₂O₄ spinel ferrites, a mixture of the same weight of CaO, CeO₂, SiO₂, nanotitania, Y₂O₃, Al₂O₃ and Bi₂O₃, in which the last one was doubled in weight, was ball milled in an agate vial and balls for an hour and then calcined at 1100 °C for 3 h, which is named MCCA.

Ni_{1-x}Zn_xFe₂O₄ (x = 0.65 and 0.70) powders were prepared via conventional ceramic technique. The appropriate stoichiometric amounts of the raw reagents were weighed according to the following chemical reaction:



where x = 0.65 and 0.70. The reagents were wet mixed in ethyl alcohol, using an agate vial and balls for 10 h in a planetary ball mill (FRITSCH P6) to get homogeneous mixtures. The mixed powders were dried at room temperature to evaporate the alcohol content. The dried powders were calcined at 1050 °C for 3 h in the air free cooling to room-temperature. The calcined powders were crushed and wet milled for 10 h, in the same conditions as mixing stage to get fine powders. After air drying, different amounts of additive (0.0, 0.5, 1.0, 1.5 and 2.0 wt%) were added to the crushed calcined powders and mixed in an agate vial for an hour using a vibrating ball mill (RETSCH, MM2 mixer mill) to obtain homogeneous mixture. Then, mixed powders were blended with 10 wt% polyvinyl alcohol (5% PVA solution) as a binder, and were formed into toroids (D_{out} = 32 mm, D_{in} = 24 mm and about 5 mm in height) using a hydraulic pressing machine under 14 ton/cm² pressure. The toroids were sintered at various temperatures (T_s), from 1150 to 1360 °C for 3 h. Heat treatment flowchart sintering is shown below:



Characterization

Phase identification of the samples was carried out with an x-ray diffractometer (BRUKER, D8 ADVANCE model) equipped with Cu tube (Cu-K α radiation, $\lambda = 1.5406 \text{ \AA}$) at a scanning rate of 0.04°/s between 20 and 80 (2 θ) degrees. Xpert High Score Plus software was used to characterized XRD patterns. Mean crystallite sizes of the powders and their strains of the crystallites were obtained by Williamson-Hall method²⁸.

$$\beta \cos \theta = \frac{0.9\lambda}{D} + 2\epsilon \sin \theta, \quad (2)$$

where λ is x-ray wavelength, θ is the Bragg angle, β is the full width at half-maximum (FWHM) that is ascribed to broadening of the crystallite size and strains, D is the mean crystallite size and ϵ is the strain. To obtain D and ϵ , a line was fitted in the $\beta \cos \theta$ with respect to $\sin \theta$ and based on the Williamson-Hall formula, y-intercept is $\frac{0.9\lambda}{D}$ and its slope equals to 2ϵ .

As the crystal structure of the samples is cubic, their lattice constants were calculated by the following relation²⁹:

$$d = \frac{a^2}{(h^2 + k^2 + l^2)^{1/2}}, \quad (3)$$

where a is the lattice constant and d is interplanar spacing of the plane with (hkl) Miller indices.

X-ray density of the samples $\rho_{x\text{-ray}}$ were calculated using the following formula³⁰:

$$\rho_{x\text{-ray}} = \frac{8M}{N_A} a^3, \quad (4)$$

where M is the formula unit weight, a is the lattice constant and N_A is the Avogadro's number.

The toroidal shape samples were wrapped by 30 turns (N) enameled copper wire and their R_s and L_s parameters were measured, using an LCR meter (Fluke, PM6303) in the frequency range of 0.1 to 1000 kHz at low magnetic flux densities. The real part of permeability (μ') and Q-factor were calculated by the following relations: $\mu' = \frac{L_s L_m}{\mu_0 N^2 A_e}$ and $Q = \frac{\omega L_s}{R_s}$, respectively, where $\omega = 2\pi f$, L_s is the series self-inductance, L_m and A_e are related to the toroids geometry by $L_m = \frac{\pi \times (D_{out} + D_{in})}{2}$ and $A_e = \frac{(D_{out} - D_{in}) \times h}{2}$, D_{out} , D_{in} and h are outer diameter, inner diameter and height of the toroids, respectively.

Result and discussion

Structural analysis

X-ray diffraction patterns of both calcined powders ($x=0.65$ and 0.70) are shown in Fig. 1(left). As can be seen, all detectable peaks are well matched with the standard spinel's peaks, which are labeled by PDF card No. 08-0234. This illustrates that single phase spinel crystal structures are mainly formed in both powders. Also a comparison between two patterns shows that all diffraction peaks related to the $x=0.70$ sample are shifted to lower diffraction angles with respect to those of the $x=0.65$ one, which is represented in Fig. 1(Right) clearly. This lead to an increase in lattice parameter based on Vegard's law³¹, which is due to substitution of larger Zn^{2+} ($R_{Zn^{2+}}$: 0.082 nm) ion for the smaller Ni^{2+} ($R_{Ni^{2+}}$: 0.072 nm) one in A sites³². Calculated lattice parameters, mean crystallite sizes, x-ray densities, lattice strains of the calcined powders and bulk densities of the sintered samples at 1250 °C are tabulated in Table 1.

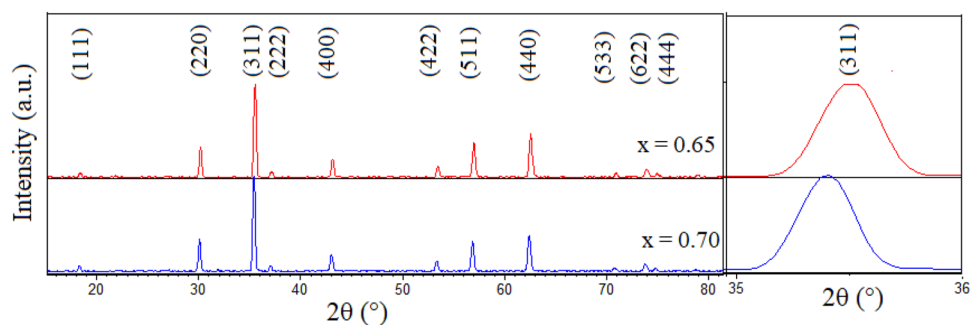


Figure 1. Left: XRD patterns of the $Ni_{1-x}Zn_xFe_2O_4$ ($x=0.65$ and 0.70) powders, calcined at 1050 °C. Right: Expanded (311) diffraction peak.

Sample	$a \pm 0.001$ (Å)	$D \pm 1$ (nm)	ϵ	$\rho_{x\text{-ray}}$ (g/cm ³)	ρ_b (g/cm ³) for $T_s = 1250$ °C
$Ni_{0.35}Zn_{0.65}Fe_2O_4$	8.393	26	0.006	5.365	4.76
$Ni_{0.3}Zn_{0.7}Fe_2O_4$	8.412	29	0.002	5.337	5.03

Table 1. Lattice parameters (a), mean crystallite sizes (D), strains (ϵ), X-ray ($\rho_{x\text{-ray}}$) and bulk (ρ_b) densities.

Permeability and Q-factor spectra

Real part of the initial permeability spectra related to the additive free $\text{Ni}_{0.35}\text{Zn}_{0.65}\text{Fe}_2\text{O}_4$ samples (sintered at 1150, 1200, 1250, 1280 and 1300 °C) and that for $\text{Ni}_{0.3}\text{Zn}_{0.7}\text{Fe}_2\text{O}_4$ samples (sintered at 1150, 1250, 1300, 1320, 1350 and 1360 °C) are presented in Fig. 2a and b, respectively.

The permeability of polycrystalline ferrites can be originated from two different magnetizing mechanisms; domain wall motion and spin rotation. The permeability follows:

$$\mu = 1 + \chi_{\text{dw}} + \chi_{\text{spin}}, \quad (5)$$

where χ_{dw} and χ_{spin} are magnetic susceptibilities of the domain wall motion and spin rotation, respectively³³. On the other hand:

$$\chi_{\text{dw}} = \frac{3\pi DM_s^2}{4\gamma}, \quad \chi_{\text{spin}} = \frac{2\pi M_s^2}{K} \quad (6)$$

where M_s is saturation magnetization, D is mean grain size, γ is domain wall energy and K is effective magnetic anisotropy constant. As domain wall motion is restricted by the grain boundaries, grains growth leads to lesser grain boundaries and then a predominant enhancement in permeability occurs^{34–37}.

Although variation of the permeability with respect to frequency for the $x=0.65$ sample (Fig. 2a) is negligible at lower sintering temperatures, but at higher ones and higher frequencies (> 100 kHz) decreases slightly. It is due to increase in Eddy current loss which is more important at higher frequencies. This restricts the applicability frequency range of the ferrites^{38,39}.

Figure 2b shows permeabilities of the $\text{Ni}_{0.3}\text{Zn}_{0.7}\text{Fe}_2\text{O}_4$ samples, sintered up to 1300 °C are relatively constant, but as can be seen the permeabilities slightly decrease, as sintering temperature increases, at frequencies greater than 100 kHz. On the other words, as sintering temperature increases utility zone decreases, which is due to grain growth⁴⁰.

To determine the effect of the sintering temperature on real part of permeability, their variations with respect to T_s were plotted in Fig. 3 at 1 kHz, which are representing values in the utility zone. As can be seen both series have maxima, which are 438 for the $x=0.65$ (sintered at 1280 °C) and 462 for $x=0.70$ (sintered at 1350 °C). The increase in permeability by increasing the sintering temperature is due to grain growth and in turn densification. The grain growth causes to decrease pores, which are domain walls' motion inhibitor. Thereby the pinning wall becomes fewer and walls move easier, which leads to higher permeability. Additionally, by increasing sintering temperature, residual stresses reduce, which in turn result in magnetic anisotropy reduction. Therefore domain wall movement facilitates and the initial permeability increases⁴¹.

As mentioned above, there is an optimum sintering temperature for each series at which the permeability is maximum. This behavior is depending on sample densification in the course of sintering. As sintering temperature increases, some Fe^{3+} ions reduce to Fe^{2+} ones and causes to make oxygen vacancies to keep charge neutrality. As Fe^{2+} ions diffuse faster than Fe^{3+} ones, thereupon grain growth turns up, which results in an increase in densification with larger grains⁴². Above optimum sintering temperature the permeability decreases which can be related to the increase in the pores within the grains in spite of increasing grain size.

Figure 4a and b show quality factors (Q-factors) spectra of the additive free sintered samples at various sintering temperature. As can be seen Q-factor of all samples raised rather rapidly with frequency showing a sharp peak and then fell, except that sintered at 1150 °C ($x=0.70$). Highest value of Q-factor for both series achieved at $T_s = 1150$ °C. The highest Q-factor of the samples at this sintering temperature may be ascribed to smaller grain size and lesser defects inside the grains than the samples sintered at higher temperatures.

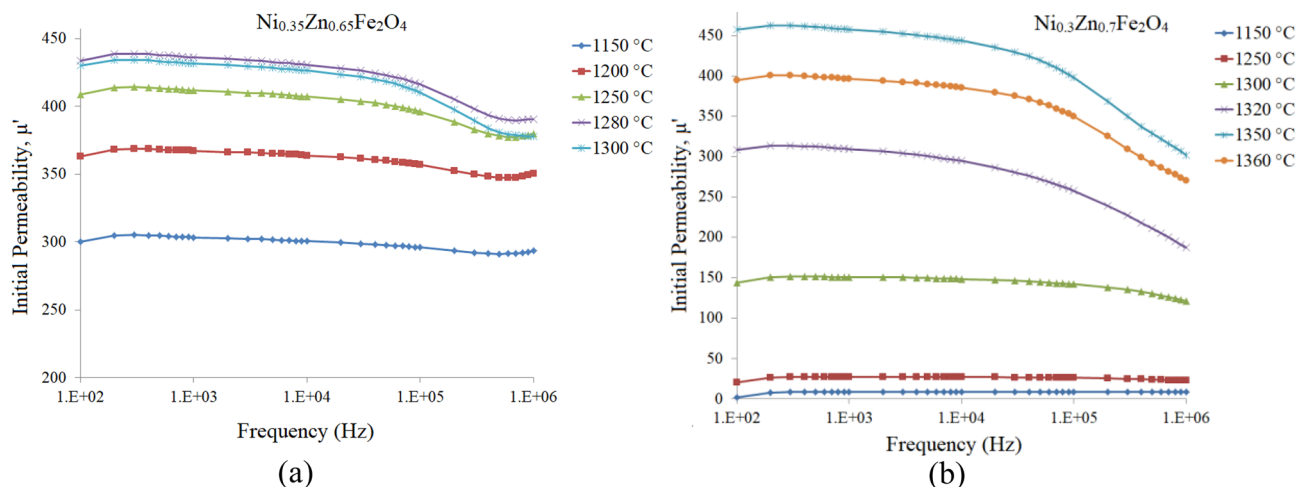


Figure 2. Real part of the initial permeability spectra for additive free (a) $\text{Ni}_{0.35}\text{Zn}_{0.65}\text{Fe}_2\text{O}_4$ and (b) $\text{Ni}_{0.3}\text{Zn}_{0.7}\text{Fe}_2\text{O}_4$ samples at different sintering temperatures.

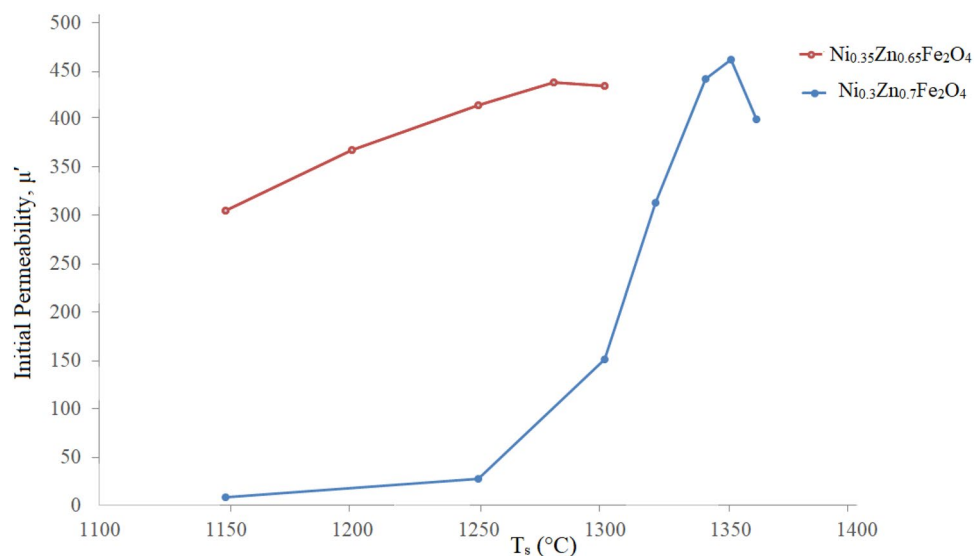


Figure 3. Variations of the real part of initial permeability (@ 1 kHz) of the additive free samples versus T_s .

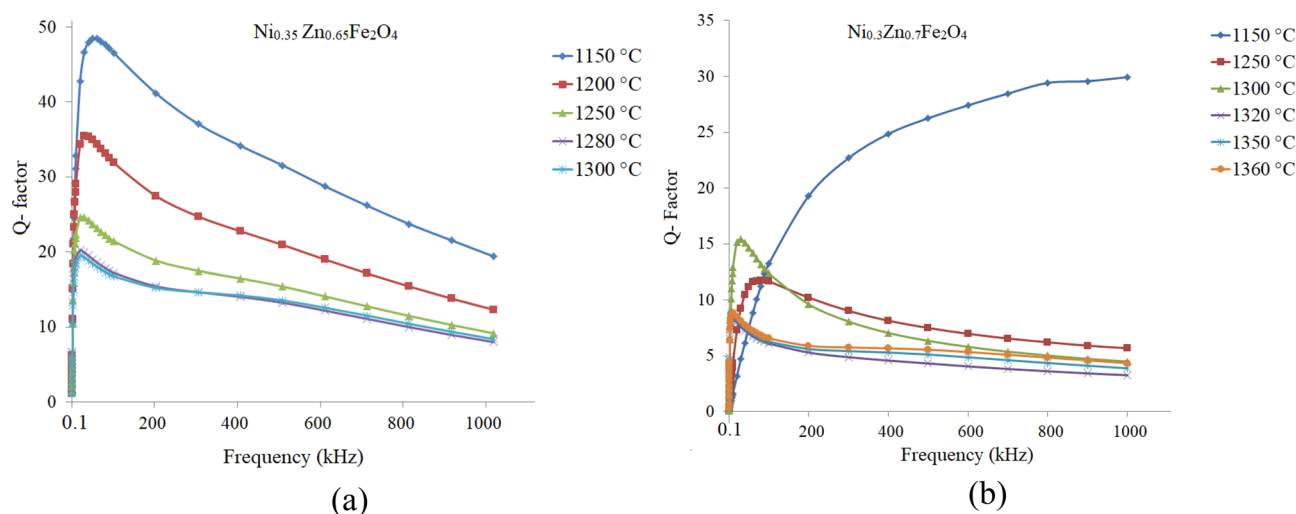


Figure 4. Q-factor spectra of the additive free samples, sintered at different temperatures: (a) $\text{Ni}_{0.35}\text{Zn}_{0.65}\text{Fe}_2\text{O}_4$, and (b) $\text{Ni}_{0.3}\text{Zn}_{0.7}\text{Fe}_2\text{O}_4$.

The effect of additive on permeability, Q- factor and sintering temperature

Figure 5a–e illustrate the initial permeability spectra of the $x = 0.65$ samples with additive (0.0–2.0 wt%) and sintered at various temperatures. As can be seen there is an optimum additive amount for each sintering temperature, Fig. 6.

As mentioned in former section variation of the initial permeability around the optimum sintering temperature, is subjected to two parameters, enhancement in grain growth and reduction in intragranular porosities. The results show that addition of additive not only enhances initial permeability, but reduces the optimum sintering temperature. As can be seen at each temperature initial permeability of the $x = 0.65$ sample with 1 wt% additive is mostly maximum and the highest value is 492 for $T_s = 1280$ °C.

Figure 7a–f show the initial permeability spectra of the $x = 0.70$ samples with additive (0.0–2.0 wt%) and sintered at various temperatures. As can be seen there is an optimum additive amount for each sintering temperature, Fig. 8.

Figure 7a ($T_s = 1150$ °C) shows that although permeabilities of the samples are low (< 10), but they are very close to each other and relatively independent of frequency. By increasing the sintering temperature to 1250 °C, additive clearly shows its marvelous effect, so the permeability increases drastically more than one order, it increases from about 8 to 134 for 1.5 wt% additive content. As can be seen by increasing sintering temperature, maximum permeability of 478 is achieved for $T_s = 1320$ °C and 0.5 wt% additive. A comparison between these results with those obtained former ($T_s = 1280$ °C, 492 and 1.0 wt% additive for $x = 0.65$) shows that there is a tight coupling between composition, sintering temperature and additive content. Therefore, optimum additive contents are 1.0

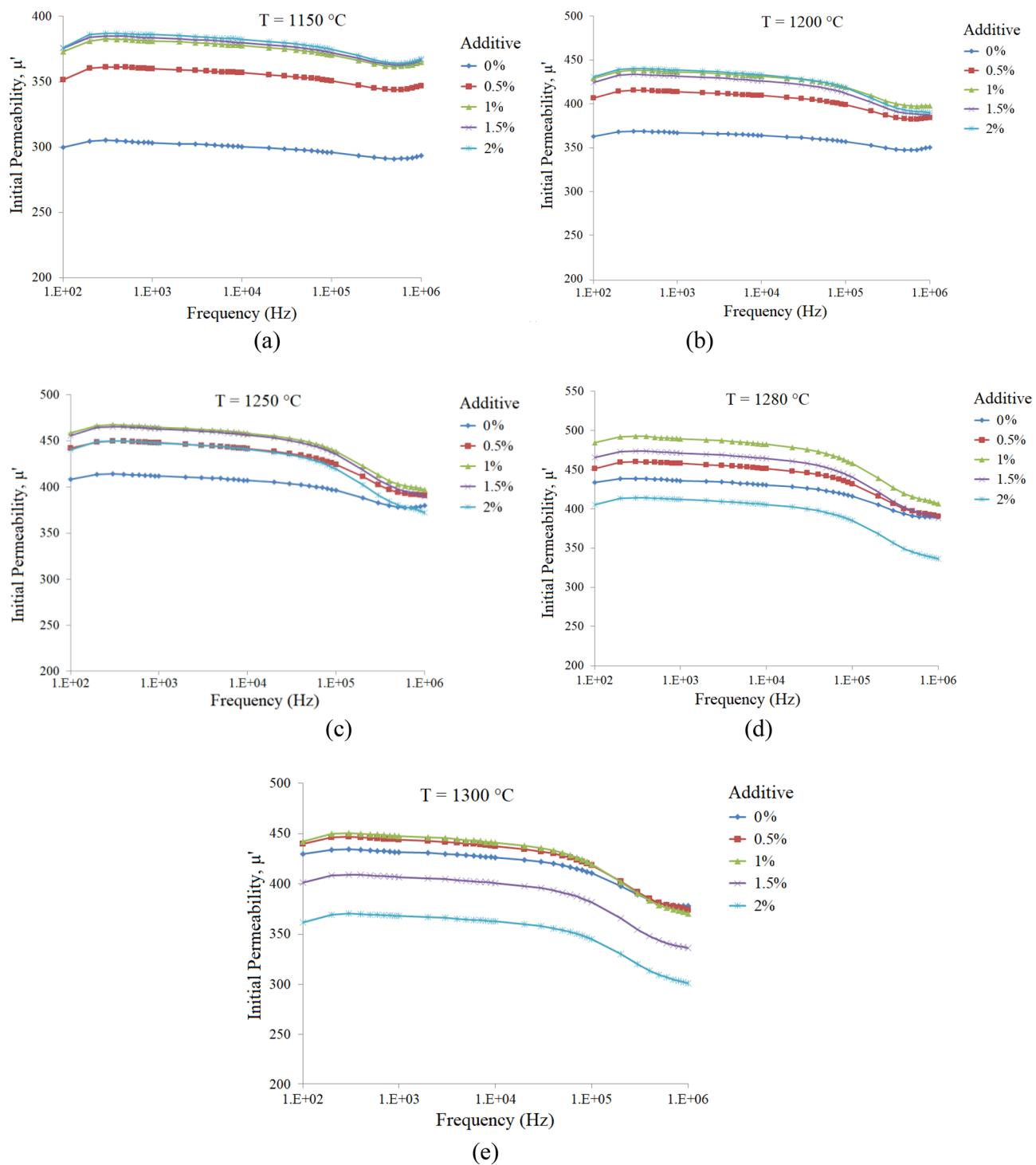


Figure 5. Initial permeability spectra of the $\text{Ni}_{0.35}\text{Zn}_{0.65}\text{Fe}_2\text{O}_4$ samples with additive (0.0–2.0 wt%) and sintered at various temperatures: (a) 1150, (b) 1200, (c) 1250, (d) 1280 and (e) 1300 °C.

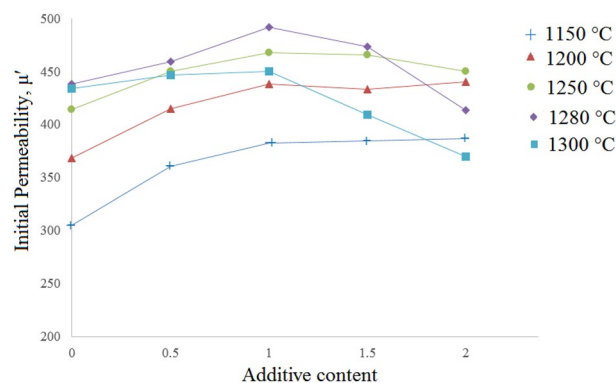


Figure 6. The variation of initial permeability (@ 1 kHz) of the $\text{Ni}_{0.35}\text{Zn}_{0.65}\text{Fe}_2\text{O}_4$ samples with respect to additive contents, sintered at various temperatures as labeled on each curve (The lines were added to guide eye).

and 0.5 wt% for $x = 0.65$ and 0.70 , respectively and this is related to the microstructure and the effect of additive on it.

The effects of additives on the microstructure of Ni–Zn ferrites can be explained by additives segregations on the grain boundaries. By the way, immigration of the grain boundaries is impeded and then preventing further crystal growth, which leads to lesser intragranular pores and absence of very large grains⁴³. Permeability spectra of the $x = 0.65$ samples with different additive contents which are sintered at various temperatures demonstrated that permeability is approximately constant at lower frequencies (< 100 kHz). The same behavior is seen for the $x = 0.70$ samples, except that the ferrimagnetic resonance occurs at lower frequencies, around 10 kHz.

Q-factor spectra of the samples with different amounts of additive that sintered at various temperatures are shown in Figs. 9a–e and 10a–f for the $x = 0.65$ and 0.70 , respectively. As can be seen, Q-factors have sharp peaks, except that related to $x = 0.70$ sintered at 1150 °C. The highest Q-factor values are belonged to the additive free samples, which may be related to smaller grain sizes and the lesser defects within the grains than those samples sintered at higher temperatures.

Conclusion

In this work nickel zinc ferrites ($\text{Ni}_{1-x}\text{Zn}_x\text{Fe}_2\text{O}_4$, $x = 0.65$ and 0.70) were prepared via conventional solid-state reaction method. Also an equiponderant mixture of Bi_2O_3 , CaO , CeO_2 , SiO_2 , Al_2O_3 , Y_2O_3 and nanotitania was calcined at 1100 °C and named multi compound calcined additive (MCCA). The MCCA causes to decrease the sintering temperature and increase the permeability remarkably in comparison with noncalcined additives. This is due to partly segregation of the calcined additive on the grain boundaries, which influences the grain boundaries' resistivity and in addition diffusion of the other parts in the spinel lattice leads to improvement magnetic properties. It can be concluded the MCCA added $\text{Ni}_{0.35}\text{Zn}_{0.65}\text{Fe}_2\text{O}_4$ is suitable for application in the switching power supplies.

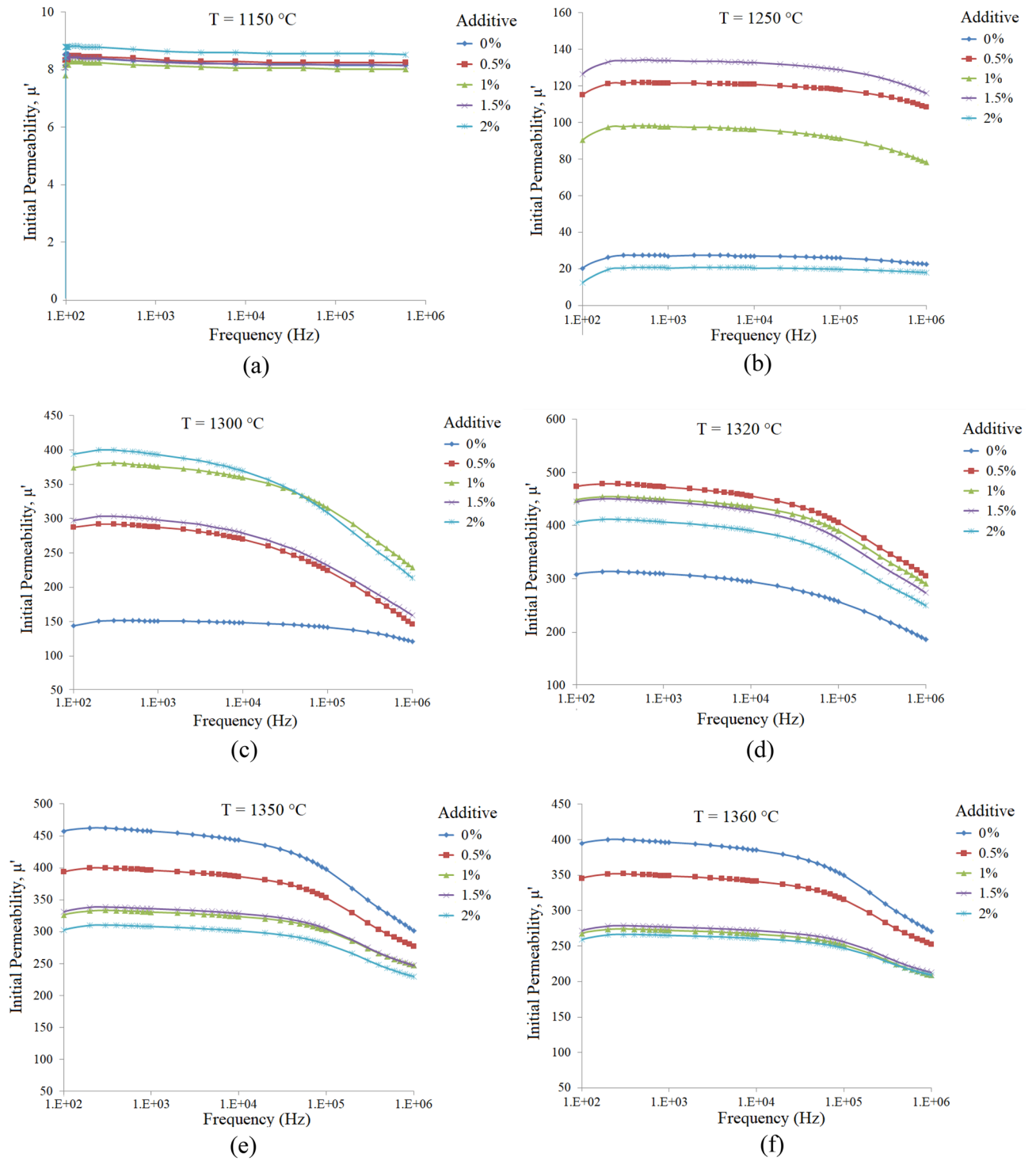


Figure 7. Initial permeability spectra of the $\text{Ni}_{0.3}\text{Zn}_{0.7}\text{Fe}_2\text{O}_4$ samples with additive (0.0–2.0 wt%) and sintered at various temperatures: (a) 1150, (b) 1250, (c) 1300, (d) 1320, (e) 1350 and (f) 1360 °C.

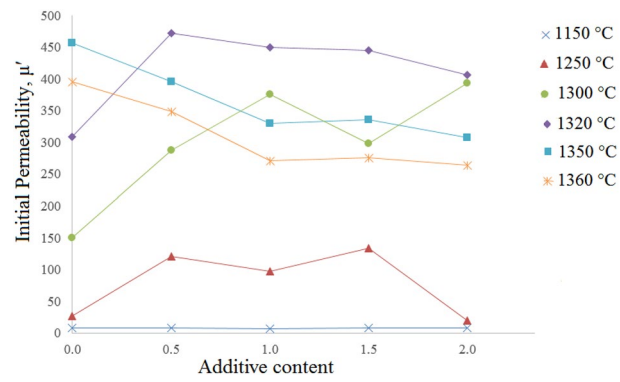


Figure 8. The variation of initial permeability (@ 1 kHz) of the $\text{Ni}_{0.35}\text{Zn}_{0.65}\text{Fe}_2\text{O}_4$ samples with respect to additive contents, sintered at various temperatures as labeled on each curve (The lines were added to guide eye).

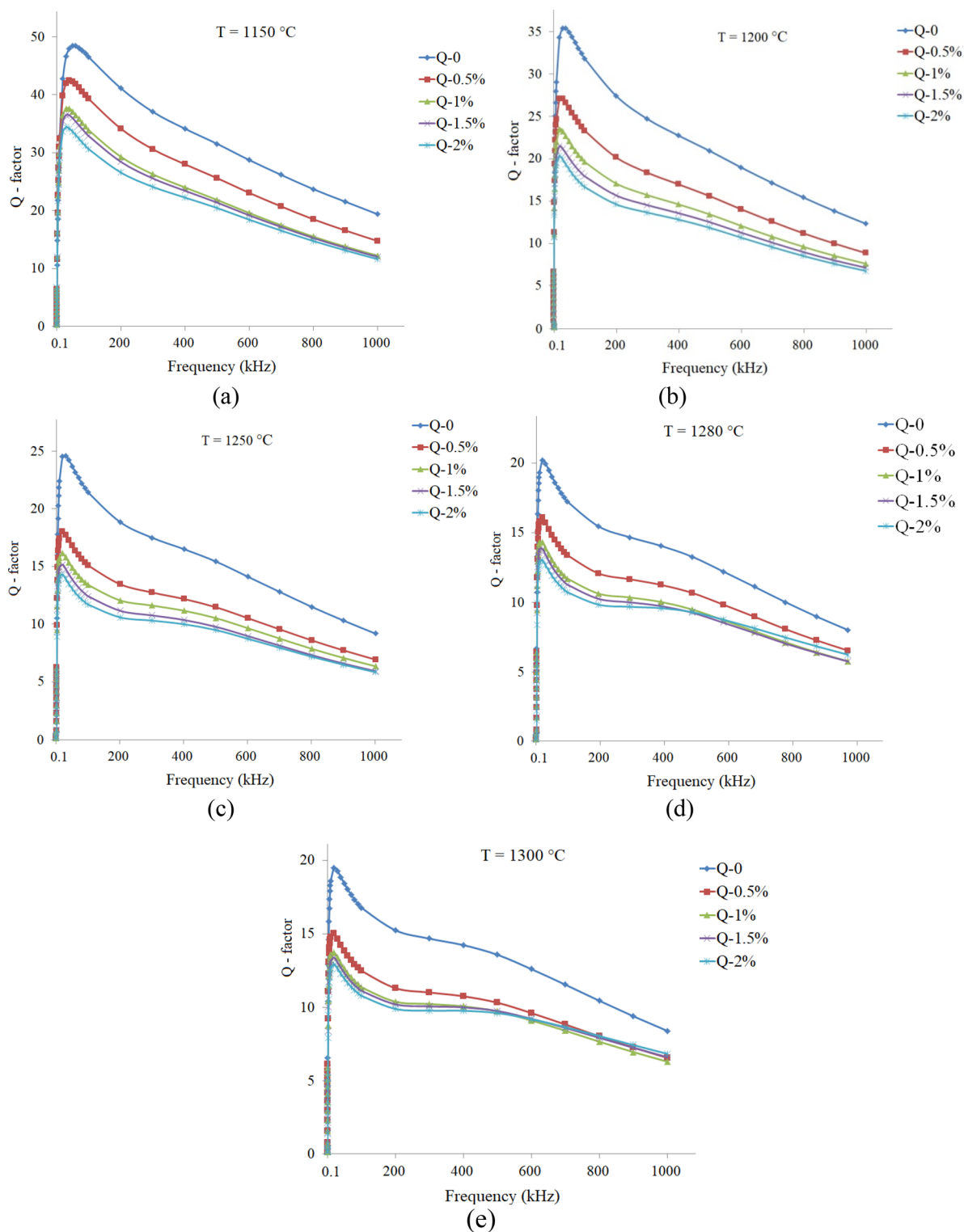


Figure 9. Q-factor spectra of the $\text{Ni}_{0.35}\text{Zn}_{0.65}\text{Fe}_2\text{O}_4$ samples with additive (0.0 up to 2.0 wt%) and sintered at various temperatures: (a) 1150, (b) 1200, (c) 1250, (d) 1280 and (e) 1300 °C.

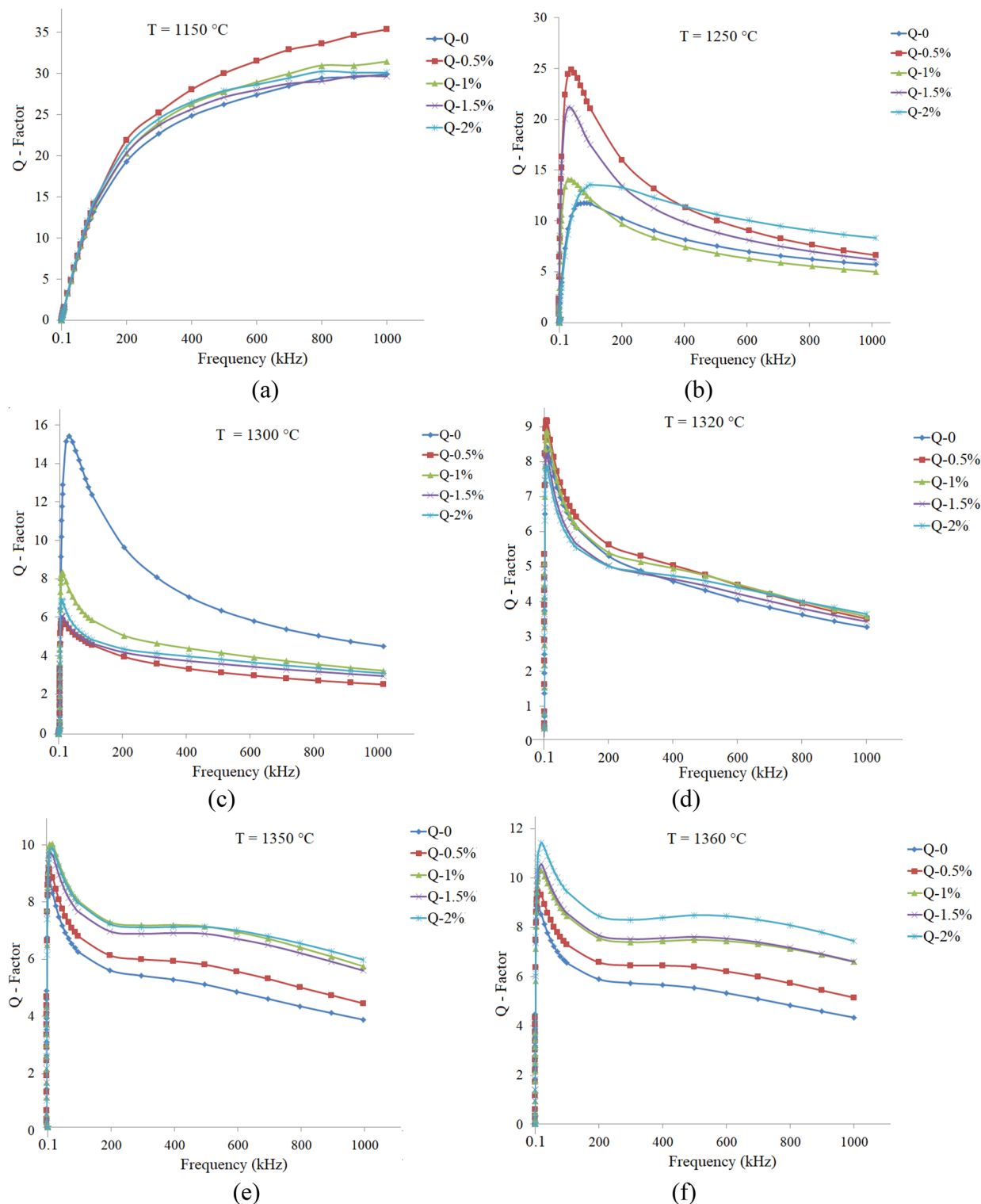


Figure 10. Q-factor spectra of the $\text{Ni}_{0.3}\text{Zn}_{0.7}\text{Fe}_2\text{O}_4$ samples with additive (0.0 up to 2.0 wt%) and sintered at various temperatures: (a) 1150, (b) 1250, (c) 1300, (d) 1320, (e) 1350 and (f) 1360 °C.

Data availability

All data generated or analyzed during this study are included in this published paper.

Received: 6 April 2024; Accepted: 4 June 2024

Published online: 06 June 2024

References

- Lyongli, *Ceramic-Matrix Composites Microstructure, Properties and Applications* (Woodhead Publishing, 2006).
- Gupta, N. & Basu, B. 10—*Hot Pressing and Spark Plasma Sintering Techniques of Intermetallic Matrix Composites* 243–302 (Elsevier, 2018).
- Nakamura, T. Snoek's limit in high-frequency permeability of polycrystalline Ni–Zn, Mg–Zn, and Ni–Zn–Cu spinel ferrites. *J. Appl. Phys.* **88**, 348–353 (2000).
- Hassan, M. *et al.* Structural parameters, energy states and magnetic properties of the novel Se-doped NiFe₂O₄ ferrites as highly efficient electrocatalysts for HER. *Ceram. Int.* **48**, 24866–24876 (2022).
- Shakirzyanov, R. I. *et al.* Impact of thermobaric conditions on phase content, magnetic and electrical properties of the CoFe₂O₄ ceramics. *J. Alloys Compd.* **954**, 170083 (2023).
- Sikder, M. S. *et al.* Improved magnetic and dielectric quality factors with low losses in rare earth (Eu) substituted Co–Ni–Zn ferrites for high frequency devices. *Results Phys.* **46**, 106320 (2023).
- Almessiere, M. A. *et al.* Impact of Eu³⁺ ion substitution on structural, magnetic and microwave traits of Ni–Cu–Zn spinel ferrites. *Ceram. Int.* **46**, 11124–11131 (2020).
- Sherstyuk, D. P. *et al.* Effect of Co content on magnetic features and SPIN states in Ni–Zn spinel ferrites. *Ceram. Int.* **47**, 12163–12169 (2021).
- Zumbahlen, H. with the engineering staff of Analog Devices, in *Linear Circuit Design Handbook, Chapter 10, Passive Components* (Elsevier, 2008).
- Derakhshani, M., Taheri-Nassaj, E., Jazirehpour, M. & Masoudpanah, S. M. Structural, magnetic, and gigahertz-range electromagnetic wave absorption properties of bulk Ni–Zn ferrite. *Sci. Rep.* **11**, 9468 (2021).
- Coey, J. M. D. *Magnetism and Magnetic Materials* (Cambridge University Press, 2009).
- Parsons, P., Duncan, K., Giri, A. K., Xiao, J. Q. & Karna, S. P. Electromagnetic properties of NiZn ferrite nanoparticles and their polymer composites. *J. Appl. Phys.* **115**, 173905 (2014).
- Trukhanov, A. V. *et al.* Influence of the dysprosium ions on structure, magnetic characteristics and origin of the reflection losses in the Ni–Co spinels. *J. Alloys Compd.* **841**, 155667 (2020).
- Derakhshani, M., Taheri-Nassaj, E., Jazirehpour, M. & Masoudpanah, S. M. Enhanced electromagnetic wave absorption performance of Ni–Zn ferrite through the added structural macroporosity. *J. Mater. Res. Technol.* **16**, 700–714 (2022).
- Kotru, S., Paul, R. & Jabera, A. Q. Synthesis and magnetic studies of pure and doped NiZn ferrite films using sol gel method. *Mater. Chem. Phys.* **276**, 125357 (2022).
- Yi, Y. *et al.* Influence of heat treatment on microstructures and magnetic properties of Fe-based soft magnetic composites prepared by co-precipitation method. *J. Magn. Magn. Mater.* **476**, 100–105 (2019).
- Song, J., Gao, Y., Tan, G., Man, Q. & Wang, Zh. Comparative study of microwave absorption properties of Ni–Zn ferrites obtained from different synthesis technologies. *Ceram. Int.* **48**, 22896–22905 (2022).
- Vicente, N., Mormeneo-Segarra, A., Clausell-Terola, C. & Barba-Juana, A. New model to tune the dielectric properties of dense and half-dense sintered polycrystalline Cu-doped Ni–Zn ferrite. *J. Eur. Ceram. Soc.* **42**, 965–972 (2022).
- El-Shater, R. E. *et al.* Synthesis, characterization, and magnetic properties of Mn nanoferrites. *J. Alloys Compd.* **928**, 166954 (2022).
- Shatooti, S. & Mozaffari, M. The effect of Zn²⁺ substitution on magnetic properties of maghemite nanoparticles, prepared by one-pot coprecipitation method at room temperature. *J. Mater. Sci. Mater. Electron.* **31**, 1891–1903 (2020).
- Darwish, M. A. *et al.* Impact of the Mg/Zn ratio on features of structural and magnetic properties in A-site stoichiometric nanosized spinel ferrites. *J. Alloys Compd.* **968**, 172278 (2023).
- Thakur, P., Taneja, Sh., Chahar, D., Ravelo, B. & Thakur, A. Recent advances on synthesis, characterization and high frequency applications of Ni–Zn ferrite nanoparticles. *J. Magn. Magn. Mater.* **530**, 167925–167945 (2021).
- Moya, J. S., Baudin, C. & Miranzo, P. *Encyclopedia of Physical Science and Technology* (Elsevier, 2003).
- Kuang, X., Carotenuto, G. & Nicolais, L. A review of ceramic sintering and suggestions on reducing sintering temperatures. *Adv. Perform. Mater.* **4**, 257–274 (1997).
- Oguntuyi, S. D., Johnson, O. T., Shongwe, M. B., Jeje, S. O. & Rominiyi, A. L. The effects of sintering additives on the ceramic matrix composite of ZrO₂: Microstructure, densification, and mechanical properties—A review. *Adv. Appl. Ceram.* **120**, 319–335 (2021).
- Zhong, X. C. *et al.* Improving soft magnetic properties of Mn–Zn ferrite by rare earth ions doping. *AIP Adv.* **8**, 047807 (2018).
- Shokrollahi, H. & Janghorban, K. Influence of additives on the magnetic properties, microstructure and densification of Mn–Zn soft ferrites. *Mater. Sci. Eng. B* **141**, 91–107 (2007).
- Williamson, G. K. & Hall, W. H. X-ray line broadening from filed aluminium and wolfram. *Acta Metall.* **1**, 22–31 (1953).
- Cullity, B. D. *Elements of X-ray Elements of X-ray Diffraction* 2nd edn. (Addison-Wesley Publishing Company, Inc, 1978).
- Smit, J. & Wijn, H. P. J. *Ferrites* 221–245 (Philips Technical Librar, y, 1959).
- Denton, A. R. & Ashcroft, N. W. Vegard's law. *Phys. Rev. A* **43**, 3161–3164 (1991).
- Rahimi, M., Kameli, P., Ranjbar, M., Hajihashemi, H. & Salamati, H. The effect of zinc doping on the structural and magnetic properties of Ni_{1-x}Zn_xFe₂O₄. *J. Mater. Sci.* **48**, 2969–2976 (2012).
- Tsutaoka, T., Ueshima, M., Tokunaga, T., Nakamura, T. & Hatakeyama, K. Frequency dispersion and temperature variation of complex permeability of Ni–Zn ferrite composite materials. *J. Appl. Phys.* **78**, 3983–3991 (1995).
- Barati, M. R. Characterization and preparation of nanocrystalline MgCuZn ferrite powders synthesized by sol–gel auto-combustion method. *J. Sol–Gel Sci. Technol.* **52**, 171–178 (2009).
- Jiang, N. N. *et al.* Influence of zinc concentration on structure, complex permittivity and permeability of Ni–Zn ferrites at high frequency. *J. Magn. Magn. Mater.* **401**, 370–377 (2016).
- Tsutaoka, T. Frequency dispersion of complex permeability in Mn–Zn and Ni–Zn spinel ferrites and their composite materials. *J. Appl. Phys.* **93**, 2789–2796 (2003).
- Mahmud, S. T. *et al.* Influence of microstructure on the complex permeability of spinel type Ni–Zn ferrite. *J. Magn. Magn. Mater.* **305**, 269–274 (2006).
- Goldman, A. *Modern Ferrite Technology* (Springer, 2006).
- Cullity, B. D. & Graham, C. D. *Introduction to Magnetic Materials* (Wiley, 2009).
- Verma, A. & Chatterjee, R. Effect of zinc concentration on the structural, electrical and magnetic properties of mixed Mn–Zn and Ni–Zn ferrites synthesized by the citrate precursor technique. *J. Magn. Magn. Mater.* **306**, 313–320 (2006).
- Jahanbin, T., Hashim, M. & Amin Mantori, K. Comparative studies on the structure and electromagnetic properties of Ni–Zn ferrites prepared via co-precipitation and conventional ceramic processing routes. *J. Magn. Magn. Mater.* **322**, 2684–2689 (2010).
- Sujatha, C., Reddy, K. R., Babu, K. S., Reddy, A. R. C. & Rao, K. H. Effect of sintering temperature on electromagnetic properties of NiCuZn ferrite. *Ceram. Int.* **39**, 1–10 (2013).
- Rezlescu, E., Rezlescu, N., Pasnicu, C., Craus, M. L. & Popa, D. P. The influence of additives on the properties of Ni–Zn ferrite used in magnetic heads. *J. Magn. Magn. Mater.* **117**, 448–454 (1992).

Acknowledgements

The authors would like to acknowledge “Deputy of Research and Technology” for financial supports.

Author contributions

This is a part of Postdoc project of Dr. S. Shatooti. The composition was designed in conjugation with Dr. M. Mozaffari and samples were prepared and measured by her. The results were analyzed commonly and first draft was prepared by Dr. S. Shatooti. M. Mozaffari reviewed the manuscript.

Competing interests

The authors declare no competing interests.

Additional information

Correspondence and requests for materials should be addressed to M.M.

Reprints and permissions information is available at www.nature.com/reprints.

Publisher's note Springer Nature remains neutral with regard to jurisdictional claims in published maps and institutional affiliations.



Open Access This article is licensed under a Creative Commons Attribution 4.0 International License, which permits use, sharing, adaptation, distribution and reproduction in any medium or format, as long as you give appropriate credit to the original author(s) and the source, provide a link to the Creative Commons licence, and indicate if changes were made. The images or other third party material in this article are included in the article's Creative Commons licence, unless indicated otherwise in a credit line to the material. If material is not included in the article's Creative Commons licence and your intended use is not permitted by statutory regulation or exceeds the permitted use, you will need to obtain permission directly from the copyright holder. To view a copy of this licence, visit <http://creativecommons.org/licenses/by/4.0/>.

© The Author(s) 2024